

Disordered Kondo-lattice model: Extension of coherent potential approximation

V. Bryksa and W. Nolting

Institut für Physik, Humboldt-Universität zu Berlin, Newtonstraße 15, Berlin D-12489, Germany

(Received 25 March 2008; published 18 August 2008)

An extension of coherent potential approximation to analyze the single-particle spectra of disordered Kondo-lattice model (KLM) to get the interconnected electronic and magnetic properties of “local-moment” systems such as diluted ferromagnetic semiconductors (DMS) is proposed. Electron scattering by the magnetic ions, which are randomly distributed over the crystal volume, is taken into account as well as the peculiarities of the exchange interaction under the single-scattering act in KLM. The coupling of the localized magnetic moments due to the itinerant electrons (holes) is treated by a modified Ruderman-Kittel-Kasuya-Yosida-theory, which maps the KLM onto an effective Heisenberg model. We discuss in detail the dependencies of the Curie temperature on the concentration x of magnetic ions, the carrier concentration n , the exchange coupling J , and the crystal-field parameters: λ^{AA} , λ^{MM} , and λ^{AM} . The latter play a crucial role for understanding and controlling the Curie temperature of DMS.

DOI: [10.1103/PhysRevB.78.064417](https://doi.org/10.1103/PhysRevB.78.064417)

PACS number(s): 75.50.Pp, 71.23.-k, 75.30.Hx, 85.75.-d

I. INTRODUCTION

There are many compounds for which we can write the formula $A_{1-x}M_x$, where A is a nonmagnetic atom and M is a magnetic atom. Such an alloy model may exhibit very rich magnetic properties, due to the exchange interaction between localized moments of the magnetic atom M and conduction-electron spin in the host of A atoms. For example, in the metallic case $\text{Cu}_{1-x}\text{Mn}_x$ (many carriers) we can study the Ruderman-Kittel-Kasuya-Yosida (RKKY) interaction and the Kondo effect.¹ In the dielectric case $\text{Ga}_{1-x}\text{Mn}_x\text{As}$ (few carriers) we have a diluted magnetic semiconductors (DMS) (Refs. 2 and 3).

The DMS materials based on III-V and II-VI semiconductors exhibit a very striking correlation between the transport and the magnetic properties.² Ideally, each Mn dopant atom represents an acceptor that introduces a local spin and a hole carrier. The ferromagnetism is driven by a charge-carrier mediated mechanism as a consequence of an interband exchange interaction between the localized magnetic moments and the carrier (hole) spins. Experimentally, the Curie temperature T_c of the DMS is enhanced by the post-growth annealing of the samples, which changes positions of defects and the hole concentration.² So the magnetism in the DMS is heavily depending on the impurity (Mn ion) disorder and dilution, carrier concentration and compensation, and the coupling mechanism between the localized Mn spins and the itinerant holes. Therefore, it is very hard to study these materials without some approximations. There are many theoretical approaches attempting to understand DMS physics.⁴⁻¹⁴ However, the mutual influence of interband coupling effects and disorder effects with respect to the ferromagnetic phase transition have not been completely understood so far. So we propose, first of all, to study the ferromagnetic properties of the ideal alloy $A_{1-x}M_x$ system.^{5,6}

As mentioned, a very important aspect of these alloys is the disorder, the magnetic and nonmagnetic atoms are distributed randomly over the crystal lattice. The magnetic exchange interactions are to be taken into account for all distances between the different moments. This defines an

effective Heisenberg model for the magnetic moments. The concentration x controls the average distance between two magnetic atoms. On the other hand, the effective Heisenberg interaction also depends on x . The same holds for interband-coupling effects.^{15,16} Both effects are important for understanding the ferromagnetic transition in such a component.^{5,6}

The most developed approach for incorporation of the carrier disorder is the coherent potential approximation (CPA).^{5,6,9,11,12,17-19} However, there are many indications that this method is not sufficient for the explanation of certain properties of the disordered ferromagnetic semiconductors.^{17,20} For example, the CPA does not incorporate the electron scattering on the crystal-field fluctuations, which are important and can change the Curie temperature very drastically.² One attempt of treating the crystal-field fluctuation in the DMS systems using numerical simulation for finite systems has recently been used in Ref. 21. However, the authors used only the effect of chemical substitution that accompanies the presence of the magnetic atom.

In this paper, we will present an approach, which is based on an extended CPA treatment that incorporates the carrier scattering on the crystal-field fluctuation (Sec. II). Numerical results concerning Curie temperatures, magnon densities of states, and effective exchange integrals are presented in Sec. III for a wide range of the model parameters such as exchange coupling J , concentration of magnetic atoms x , electron band occupation n , and temperature T . Section IV is assigned to a summary and an outlook.

II. SELF-CONSISTENT CALCULATION OF THE ELECTRON SPECTRUM

The Hamiltonian of the disordered Kondo-lattice model (KLM) for the $A_{1-x}M_x$ alloy can be written in second-quantized form as a sum of a kinetic energy, an exchange interaction, and a crystal-field energy:⁶

$$\hat{H} = \sum_{i,j,\sigma} t_{ij} a_{i\sigma}^{\dagger} a_{j\sigma} + \sum_i \hat{H}_i, \quad (1)$$

where the single-site part \hat{H}_i has the following form:

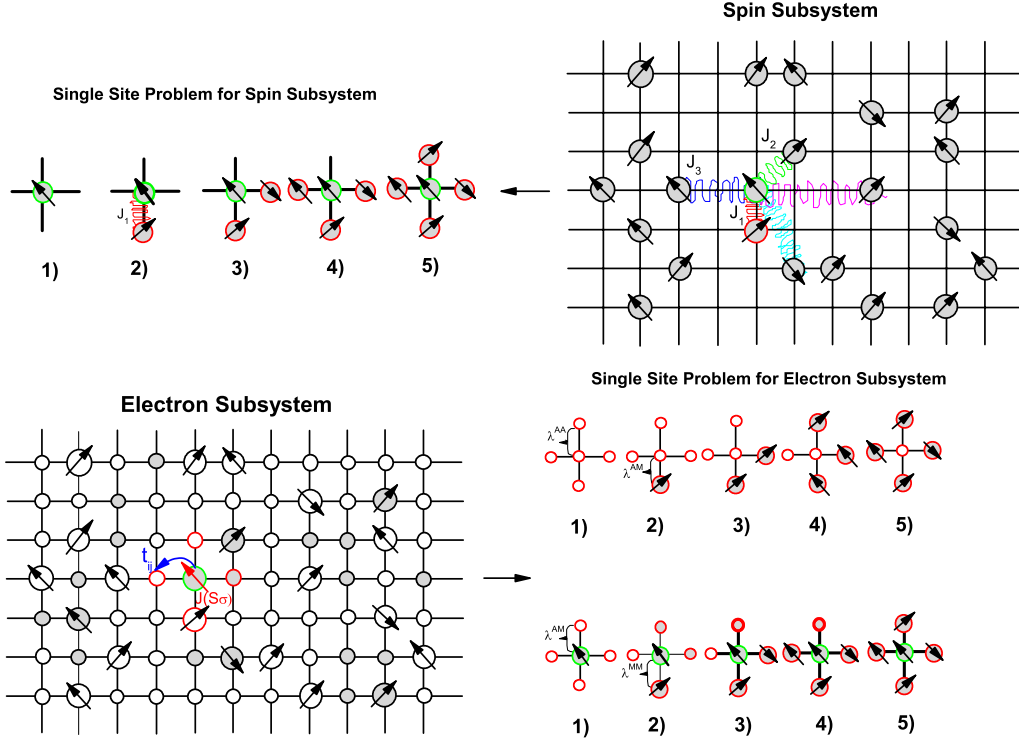


FIG. 1. (Color online) General procedure of the self-consistent mapping of the disordered Kondo-lattice model onto disordered Heisenberg model

$$\hat{H}_i = \sum_{\sigma} \epsilon_i n_{i\sigma} + \sum_{\sigma, \sigma'} J_i(\vec{S}_i \vec{\sigma})_{\sigma\sigma'} a_{i\sigma}^{\dagger} a_{i\sigma'} + \sum_{\sigma} \delta L_i n_{i\sigma}. \quad (2)$$

$a_{i\sigma}^{\dagger}$ ($a_{i\sigma}$) is the creation (annihilation) operator for the Wannier electron with the spin σ ($\sigma = \uparrow, \downarrow$) at the site \vec{R}_i . In order to introduce the disorder into the $A_{1-x}M_x$ KLM, we introduce projection operators;

$$X_i^A = \begin{cases} 1, & \text{- if site } i \text{ is } A \\ 0, & \text{- otherwise,} \end{cases} \quad (3)$$

$$X_i^M = \begin{cases} 1, & \text{- if site } i \text{ is } M \\ 0, & \text{- otherwise.} \end{cases} \quad (4)$$

The energy and exchange coupling constants are written as

$$\epsilon_i = \sum_{k \in A, M} \epsilon^k X_i^k, \quad (5)$$

$$J_i = \sum_{k \in A, M} J^k X_i^k,$$

where chemical energy parameters $\epsilon^A = \epsilon^M = 0$ are equivalent, and exchange couplings are $J^M = J$ and $J^A = 0$ for magnetic and nonmagnetic atoms, respectively.

The crystal-field energy is given by

$$\delta L_i = \sum_{k \in A, M} \sum_{l \in A, M} \sum_{j \neq i} X_i^k \lambda_{ij}^{kl} X_j^l,$$

$$\lambda_{ij}^{kl} = \int \varphi_{ki}^*(\vec{r}) U_l(\vec{r} - \vec{R}_j) \varphi_{kl}(\vec{r}) d\vec{r}, \quad (6)$$

where the $U_l(\vec{r} - \vec{R}_j)$ term is the potential energy of the electron at the point \vec{r} near the site defined by the radius vector \vec{R}_j . The cluster wave functions φ_{ki} are constructed from the atomic functions of an i site of k type.

The transfer matrix is written as

$$t_{ij} = \sum_{k, k' \in A, M} t^{kk'} X_i^k X_j^{k'}, \quad (7)$$

where hopping parameters $t^{AA} = t^{MM} = t^{AM} = t^{MA} = t = W/6$ are the same for the different kind of atoms and are equal to the half bandwidth W for the case of simple cubic lattice.

To study conduction-electron properties, we use the configurationally averaged single-electron Green's function,^{17,18}

$$G_{ij\sigma}(E) = \overline{\langle \langle a_{i\sigma} | a_{j\sigma}^{\dagger} \rangle \rangle_E}. \quad (8)$$

We introduce the symbol $\overline{(\dots)}$ to denote the configurational ensemble average.

The relation between the band occupation n and the chemical potential μ is as follows:

$$n = n_{\uparrow} + n_{\downarrow} = -\frac{1}{\pi} \sum_{\sigma} \int_{-\infty}^{\infty} \frac{\text{Im } G_{ii,\sigma}(E)}{e^{\beta(E-\mu)} + 1} dE, \quad (9)$$

with $\beta = 1/kT$ as the inverse temperature.

We use the idea of mapping the disordered KLM on an effective random spin Heisenberg Hamiltonian^{5,6,15} (see Fig. 1);

$$\hat{H}^{RH} = -\frac{1}{2} \sum_{ij} J_{ij} X_i^M X_j^M (S_i^z S_j^z + S_i^+ S_j^-), \quad (10)$$

where J_{ij} is an effective interaction between localized magnetic moments. If we assume that we can calculate the effective interaction J_{ij} within the frame of the modified RKKY-method (MRKKY) (Refs. 15 and 19),

$$J_{\vec{q}} = \frac{J^2}{4\pi} \int \frac{dE}{e^{\beta(E-\mu)} + 1} \frac{1}{N} \sum_{\sigma, \vec{k}} \text{Im}[G_{\vec{k}}^0(E) G_{\vec{k}+\vec{q}, \sigma}(E)], \quad (11)$$

where $J_{\vec{q}}$ is the Fourier transform of J_{ij} , then we get the self-consistent loop for a finite temperature calculation (see more detail in Ref. 6). In order to study magnetic properties of the disordered KLM, we calculate the configurationally averaged magnon Green's function;

$$D_{\vec{q}}(E) = \overline{\langle\langle S_{\vec{q}}^+ | S_{-\vec{q}}^- \rangle\rangle_E}. \quad (12)$$

By use of the Callen equation²² it is then possible to calculate the magnetization $\langle S^z \rangle$:

$$\langle S^z \rangle = \frac{(S - \phi)(1 + \phi)^{2S+1} + (S + 1 + \phi)\phi^{2S+1}}{(1 + \phi)^{2S+1} - \phi^{2S+1}}, \quad (13)$$

where

$$\phi = -\frac{1}{\pi} \frac{1}{N} \sum_{\vec{q}} \int_0^\infty \frac{\text{Im} D_{\vec{q}}(E)}{e^{\beta E} - 1} dE. \quad (14)$$

So, we have a model with two subsystems (Fig. 1), and the disorder in the two subsystems plays a different role.

For the spin subsystem we restrict ourselves here to the simple virtual crystal approximation (VCA) that includes only the clusters (1) and (5) in Fig. 1. This is exclusively done because of mathematical simplicity. Since the main focus of the present study is on the influence of crystal-field effects appearing in the electronic subsystem, only, VCA for the spin system may be sufficient. An alternative approach would be the so-called low-quadratic approximation (LQA) (see Ref. 23) by which we investigated in our previous paper (Ref. 6) the disorder in the spin subsystem. With respect to the disorder problem of the electron subsystem, there are many papers^{5,6,9,11,12,17-19} using the CPA technique to find the electron spectrum for a random crystal. But the CPA includes only clusters (1) and (5) on Fig. 1. The idea to include crystal-field effects ($\lambda^{AA}, \lambda^{AM}, \lambda^{MM}$) into the Hamiltonian [Eq. (1)] can improve this CPA ansatz. It is clear that we have to use the cluster CPA technique for the disordered electronic part. Now we discuss this approximation in more detail.

A. Electron subsystem: Cluster CPA treatment

Since the introduction of diagrammatic notation by Edwards²⁴ for classifying and collecting the terms in the perturbation expansion of the electronic properties of alloys, many authors have extensively used such diagrams to study many properties of disordered systems,¹⁷ and they have been useful in seeing what sorts of scattering are physically important.

We shall use this method to obtain the CPA equations as a self-consistent scattering problem, but shall begin our description by writing the series of diagrams for the Green's function $\langle\langle a_{i\sigma} | a_{j\sigma}^+ \rangle\rangle_E$ before the configurational ensemble average procedure [Eq. (8)]. For the alloy $A_{1-x}M_x$, the perturbations are the interatomic hopping t_{ij} [Eq. (7)] and crystal-field coupling δL_i [Eq. (6)].

$$\langle\langle a_{i\uparrow} | a_{j\uparrow}^+ \rangle\rangle_E = \text{---} \overset{\circ}{\leftarrow} \text{---} + \text{---} \overset{\circ}{\leftarrow} \text{---} \overset{\circ}{\leftarrow} \text{---} + \text{---} \overset{\circ}{\leftarrow} \text{---} \overset{\circ}{\leftarrow} \text{---} \overset{\circ}{\leftarrow} \text{---} + \dots \quad (15)$$

$$\text{---} \overset{\circ}{\leftarrow} \text{---} = \text{---} \overset{\circ}{\leftarrow} \text{---} + \text{---} \overset{\circ}{\leftarrow} \text{---} \overset{\circ}{\leftarrow} \text{---} + \text{---} \overset{\circ}{\leftarrow} \text{---} \overset{\circ}{\leftarrow} \text{---} \overset{\circ}{\leftarrow} \text{---} + \dots \quad (16)$$

The graphical symbols refer to

$$\text{---} \overset{\circ}{\leftarrow} \text{---} \equiv \delta_{ij} g_{i\uparrow}(E) = \delta_{ij} \sum_k g_{i\uparrow}^k(E) X_i^k, \quad (17)$$

the electron local propagator near the site i for the spin \uparrow ;

$$\overset{\circ}{\circ} \text{---} \equiv \delta L_i \quad (18)$$

the crystal-field perturbation on the site i from the neighbor atoms;

$$\overset{i}{\sim} \overset{j}{\sim} \equiv t_{ij} \quad (19)$$

the transfer matrix between two neighbor sites i and j .

An open arrow (full arrow) on the horizontal electron line means an electron with spin up (down). The same we can write down for the \downarrow Green's function $\langle\langle a_{i\downarrow} | a_{j\downarrow}^+ \rangle\rangle_E$. The hopping and crystal-field perturbations do not change the spin quantum number σ in the electron scatterings.

For the electron local propagator $g_{i\sigma}^k(E)$ we have the Dyson equation;

$$g_{i\sigma}^k(E) = \frac{1}{E - \epsilon^k - \Sigma_{\sigma}^k(E)}, \quad (20)$$

where the self-energy $\Sigma_{\sigma}^k(E)$ describes the electronic properties of the itinerant electron subsystem in the diluted ferromagnetic alloy $A_{1-x}M_x$. The local self-energy is approximately negligible for nonmagnetic atoms ($k=A$) and contains two electron spin scattering parts (Ising and spin-flip parts) for magnetic atoms ($k=M$). The local electronic self-energy $\Sigma_{\sigma}^k(E)$ becomes the central quantity of the many-body problem. For finite temperatures and arbitrary band occupations, an exact expression of $\Sigma_{\sigma}^k(E)$ is not available and one needs to apply an approximation. In this paper, we use the interpolating self-energy approach (ISA) (Ref. 19), which results in a wave-vector independent self-energy $\Sigma_{\sigma}^k(E)$, and is presented in the Appendix

$$\Sigma_{\sigma}^k(E) = \begin{cases} 0, & \text{if } k=A \\ \sum_{\sigma}^{\text{ISA}}(E), & \text{if } k=M \end{cases}. \quad (21)$$

After summation the set of diagrams [Eq. (16)] reduces to the electron local propagator renormalized by the crystal-field effect;

$$\text{---}\overset{\circ}{\text{---}} = \delta_{ij} \sum_k \frac{X_i^k}{[g_{i\uparrow}^k(E)]^{-1} + \delta L_i^k}. \quad (22)$$

In order to perform the averaging over the X operator in the electron Green's function $\langle\langle a_{i\sigma} | a_{j\sigma}^+ \rangle\rangle_E$, the density operator $\hat{\rho}_X$ can be written as

$$\hat{\rho}_X = \prod_i \rho_X^i = \prod_i [(1-x)X_i^A + xX_i^M]. \quad (23)$$

For example, using the density operator, one gets the averaged $\langle X_i^k \rangle$ operators and the electron local propagator $\langle g_{\sigma i} \rangle_X$;

$$\langle X_i^k \rangle_X = \text{Tr}_X(X_i^k \hat{\rho}_X) = \begin{cases} 1-x, & k=A \\ x, & k=M \end{cases}, \quad (24)$$

$$\langle g_{\sigma i} \rangle_X = \text{Tr}_X(g_{\sigma i} \hat{\rho}_X) = (1-x)g_{\sigma i}^A + xg_{\sigma i}^M.$$

For averaging of the Green's function [Eq. (15)], we use the standard cumulant decompositions.^{17,18} The cumulants of two random variables $g_{\sigma i}$ and δL_i are defined by

$$S^\sigma(\zeta_1; \zeta_2) = \langle e^{\zeta_1 g_{\sigma i} + \zeta_2 \delta L_i} \rangle = \exp\left(\sum_{n,m;n+m>0} \frac{[\zeta_1]^n [\zeta_2]^m}{n! m!} M_{nm}^\sigma \right), \quad (25)$$

where ζ_1, ζ_2 are infinitesimal variables.

From that it follows the cumulant expression;^{17,18}

$$M_{nm}^\sigma = \frac{\partial^n}{\partial \zeta_1^n} \frac{\partial^m}{\partial \zeta_2^m} S^\sigma(\zeta_1 \rightarrow 0; \zeta_2 \rightarrow 0). \quad (26)$$

In the graphical presentation, the cumulant is shown as oval near given site. For example, the first electron cumulant near one local electron line $g_{\uparrow i}$ and one crystal-field point δL_i and the second electron cumulant near two local electron lines gather one and two separate parts, respectively,

$$\text{---}\overset{\circ}{\text{---}} \equiv M_{10}^\uparrow = (1-x)g_{\uparrow i}^A + xg_{\uparrow i}^M,$$

$$\text{---}\overset{\circ}{\text{---}} \equiv M_{20}^\uparrow = -(M_{10}^\uparrow - g_{\uparrow i}^A)(M_{10}^\uparrow - g_{\uparrow i}^M),$$

$$\text{---}\overset{\circ}{\text{---}} \equiv M_{01}^\uparrow = M_{01}^\downarrow = \langle \delta L_i \rangle_X. \quad (27)$$

In this study we consider solely the diagrams for which the configuration averaging embraces the electron propagators and the crystal field separately. Such averaging is equivalent to the statement of the coherent potential to be independent of the crystal field. The local Green's functions [Eq. (16)] become renormalized by crystal field, but new poles do not arise. Therefore, it is appropriate to introduce a special notation of such renormalized Green's function [first diagram in the expression (15)];

$$\text{---}\overset{\circ}{\text{---}} = \text{---}\overset{\circ}{\text{---}} \equiv \langle g_{\sigma i}(E) \rangle_X. \quad (28)$$

The configuration averaging of each line in Eqs. (16) and (28) can be performed in different ways,^{25,26} but in this paper we use the cluster approximation.²⁵ In the cluster approach one has:

$$D_{i\sigma}^k(E) \equiv \left\langle \frac{1}{[g_{\sigma i}^k(E)]^{-1} - \delta L_i} \right\rangle_X$$

$$= \sum_{r=0}^z \frac{w(r)}{r! [g_{\sigma i}^k(E)]^{-1} - (z-r)\lambda_{ij}^{kk} - r\lambda_{ij}^{kk'}}, \quad (29)$$

where $w(r) = z! / [r!(z-r)!] (1-x)^r x^{z-r}$; $k' \neq k$; z is the number of nearest neighbors; i and j are the nearest-neighbors sites in the crystal lattice.

The further averaging over the full Green's function $\langle\langle a_{i\uparrow} | a_{j\uparrow}^+ \rangle\rangle_E$ in the Eq. (15) leads to the equation for the averaged Green's function,

$$G_{\sigma,ij}(E) = \Xi_{\sigma,ij}(E) + \sum_{i_1, j_1} \Xi_{\sigma,ii_1}(E) t_{i_1 j_1} G_{\sigma, j_1 j}(E). \quad (30)$$

Here the $\Xi_{\sigma,ij}$ term is the self-energy part of the averaged Green's function in the Larkin presentation for whole crystal and is irreducible by the transfer. It is called the locator in Ref. 17 and has the following diagram representation:

$$\Xi_{\sigma,ij} = \text{---}\overset{\circ}{\text{---}} + \text{---}\overset{\circ}{\text{---}} + \text{---}\overset{\circ}{\text{---}} + \dots \quad (31)$$

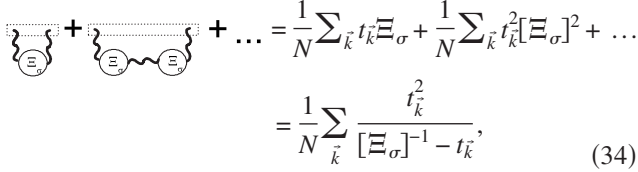
Let us restrict ourselves to single-site diagrams in the $\Xi_{\sigma,ij}$ expression (31) (e.g., 1, 2, 3, and so on), i.e., to the single-site approximation $\Xi_{\sigma,ij}(E) = \delta_{ij} \Xi_{\sigma}(E)$. Then Eq. (31) can be rewritten in the form:

$$\Xi_{\sigma} = \text{---}\overset{\circ}{\text{---}} + \text{---}\overset{\circ}{\text{---}} + \text{---}\overset{\circ}{\text{---}} + \dots \quad (32)$$

where $J_{\sigma}(E)$ is the sum of all diagrams beginning and terminating at the same site and having no common cumulants. The set [Eq. (32)] can be calculated using the technique of Ref. 17.

$$\Xi_{\sigma}(E) = \frac{(1-x)D_{\sigma}^A(E) + xD_{\sigma}^M(E) - D_{\sigma}^A(E)D_{\sigma}^M(E)J_{\sigma}(E)}{1 - [xD_{\sigma}^A(E) + (1-x)D_{\sigma}^M(E)]J_{\sigma}(E)}. \quad (33)$$

On the other hand, the sum $J_{\sigma}(E)$ can be determined if one finds the sum of all diagrams beginning and terminating at the same site and having the common cumulants (ovals);



$$\begin{aligned} \text{Diagram 1} + \text{Diagram 2} + \dots &= \frac{1}{N} \sum_{\vec{k}} t_{\vec{k}} \Xi_{\sigma} + \frac{1}{N} \sum_{\vec{k}} t_{\vec{k}}^2 [\Xi_{\sigma}]^2 + \dots \\ &= \frac{1}{N} \sum_{\vec{k}} \frac{t_{\vec{k}}^2}{[\Xi_{\sigma}]^{-1} - t_{\vec{k}}}, \end{aligned} \quad (34)$$

where $t_{\vec{k}}$ is the Fourier transform of the transfer matrix. It is clear that the sum Eq. (34) (called the fully renormalized interactor in Ref. 17) is equal to

$$\frac{1}{N} \sum_{\vec{k}} \frac{t_{\vec{k}}^2}{[\Xi_{\sigma}(E)]^{-1} - t_{\vec{k}}} = \frac{J_{\sigma}(E)}{1 - \Xi_{\sigma}(E)J_{\sigma}(E)}. \quad (35)$$

Let us rewrite the expressions (30), (34), and (35) in the form of the equations for the coherent potential as follows:

$$G_{\sigma,ii}(E) = \frac{1}{N} \sum_{\vec{k}} \frac{1}{[\Xi_{\sigma}(E)]^{-1} - t_{\vec{k}}}. \quad (36)$$

Then the coherent potential $J_{\sigma}(E)$ takes the form,

$$J_{\sigma}(E) = [\Xi_{\sigma}(E)]^{-1} - [G_{\sigma,ii}(E)]^{-1}. \quad (37)$$

Combining Eqs. (33), (36), and (37) one gets the solution of the self-consistent problem for the $A_{1-x}M_x$ crystal lattice

$$\begin{aligned} G_{\sigma,ii}(E) &= \frac{1-x}{[D_{\sigma}^A(E)]^{-1} - [\Xi_{\sigma}(E)]^{-1} + G_{\sigma,ii}^{-1}(E)} \\ &+ \frac{x}{[D_{\sigma}^B(E)]^{-1} - [\Xi_{\sigma}(E)]^{-1} + G_{\sigma,ii}^{-1}(E)}, \end{aligned} \quad (38)$$

where the disorder in the first coordination sphere (see Fig. 1) is included in the local propagators $D_{\sigma}^A(E)$ and $D_{\sigma}^B(E)$, which can be evaluated by using the cluster approach [Eq. (29)].

B. Magnetic subsystem: Virtual crystal approach

This is the most simplest approximation for the magnon Green's function.⁶ If we neglect all magnon scattering processes on the disorder, we obtain the following expression for the magnon Green's function:

$$\langle\langle S_{\vec{q}}^+ | S_{\vec{q}'}^- \rangle\rangle_E = \delta(\vec{q} + \vec{q}') \frac{2x \langle S^z \rangle}{E - 2x \langle S^z \rangle [J(0) - J(\vec{q})]}. \quad (39)$$

C. Full self-consistent approach

This technique was described in recent papers^{5,6} and is schematically illustrated in Fig. 1 and proceeds as follows. For the zero temperature and for the saturated magnetization $\langle S^z \rangle = S$, the electronic part of the model Hamiltonian is solved by using a single-particle Green's function [Eq. (38)], where the crystal-field parameters ($\lambda^{AA}, \lambda^{AM}, \lambda^{MM}$) are included in the average local Green's function [Eq. (29)]. The result provides the single-site self-energy $\Xi_{\sigma}(E)$ for a given band occupation of the conduction band n [Eq. (9)], concentration of the magnetic atoms x , and exchange coupling constant J . In order to study the magnetic properties (finite tem-

perature), we use the MRKKY theory that results from mapping the s - f interaction onto an effective Heisenberg model. Getting effective exchange integrals J_{ij} [Eq. (11)] is mainly determined by the electronic self-energy. Finally, considering random distribution of the magnetic ions, the effective Heisenberg model [Eq. (10)] is solved in the cluster CPA framework⁶ self-consistently and new magnetization $\langle S^z \rangle$ can be derived from the magnon Green's function in the VCA approximation [Eqs. (12) and (39)] and the Callen equation [(13)]. The entire procedure is repeated until the solution of $\langle S^z \rangle$ is self-consistent. Furthermore, one can change the temperature and repeat the entire $\langle S^z \rangle$ self-consistent calculation until one gets $T_c(\langle S^z \rangle = 0)$.

III. RESULTS AND CALCULATION

We have evaluated our theory for a local-moment system ($S=5/2$) on a simple-cubic lattice with the width of the free Bloch band to be $2W=1$ eV and for a small electron concentration n . We are interested in how disorder (dilution case $\lambda=0$ and cluster effects $\lambda \neq 0$) of the localized moments influence the electronic and magnetic properties of the system. We start with the inspection of the electronic part in terms of the quasiparticle density of states (DOS).

Figure 2 shows the quasiparticle DOS of the conduction band at $T=0$ for two different cases: switch off ($\lambda^{AA}=0, \lambda^{AM}=0, \lambda^{MM}=0$) and switch on ($\lambda^{AA} \neq 0, \lambda^{AM} \neq 0, \lambda^{MM} \neq 0$) the crystal-field effects. In the first case the properties of the disordered Kondo-lattice are absolutely the same as was discussed in the earlier papers.^{5,6,12} The DOSs consist of two correlated and one noncorrelated bands per spin direction. The correlated bands correspond to the magnetic atoms M , with the spectral weight $\sim x$ and the center of gravity ϵ_M . The noncorrelated band stems from nonmagnetic atoms A with the spectral weight $\sim (1-x)$ and the center of gravity ϵ_A . The DOS of the correlated bands for $\langle S^z \rangle = S(T=0)$ and a large enough interband exchange coupling J consists in general of two subbands centered near the atomic energies: $-JS/2$ and $J(S+1)/2$. For the spin-up electrons at $T=0$ there is no DOS for energies around $J(S+1)/2$, while the spin-down density is finite there (magnetic polaron states). For weak couplings ($J < 0.2$) correlated and uncorrelated bands are mixed preventing a clear interpretation of the various influences. For the electron DOS with the crystal-field effects included, these two bands are built-up by seven minibands, which correspond to the cluster types presented in Fig. 1. The denominator of the local Green's function [Eq. (29)] controls the center of gravity of every miniband and the numerator controls the shape of the minibands. Figure 2 presents the influence of different crystal-field parameters ($\lambda^{AA}, \lambda^{AM}, \lambda^{MM}$) on the electron DOS. At very low x , the crystal field between two neighbor nonmagnetic atoms λ^{AA} cannot change (shift) the DOS very drastically and the electron DOS (red line) is approximately the same as the DOS without the crystal-field effects (black line). Increasing the crystal-field parameter λ^{MM} between two magnetic atoms, the center of gravity of the correlated subband monotonically shifts to higher energy hardly changing the noncorrelated bands (blue line on Fig. 2). The crystal field between magnetic and nonmagnetic at-

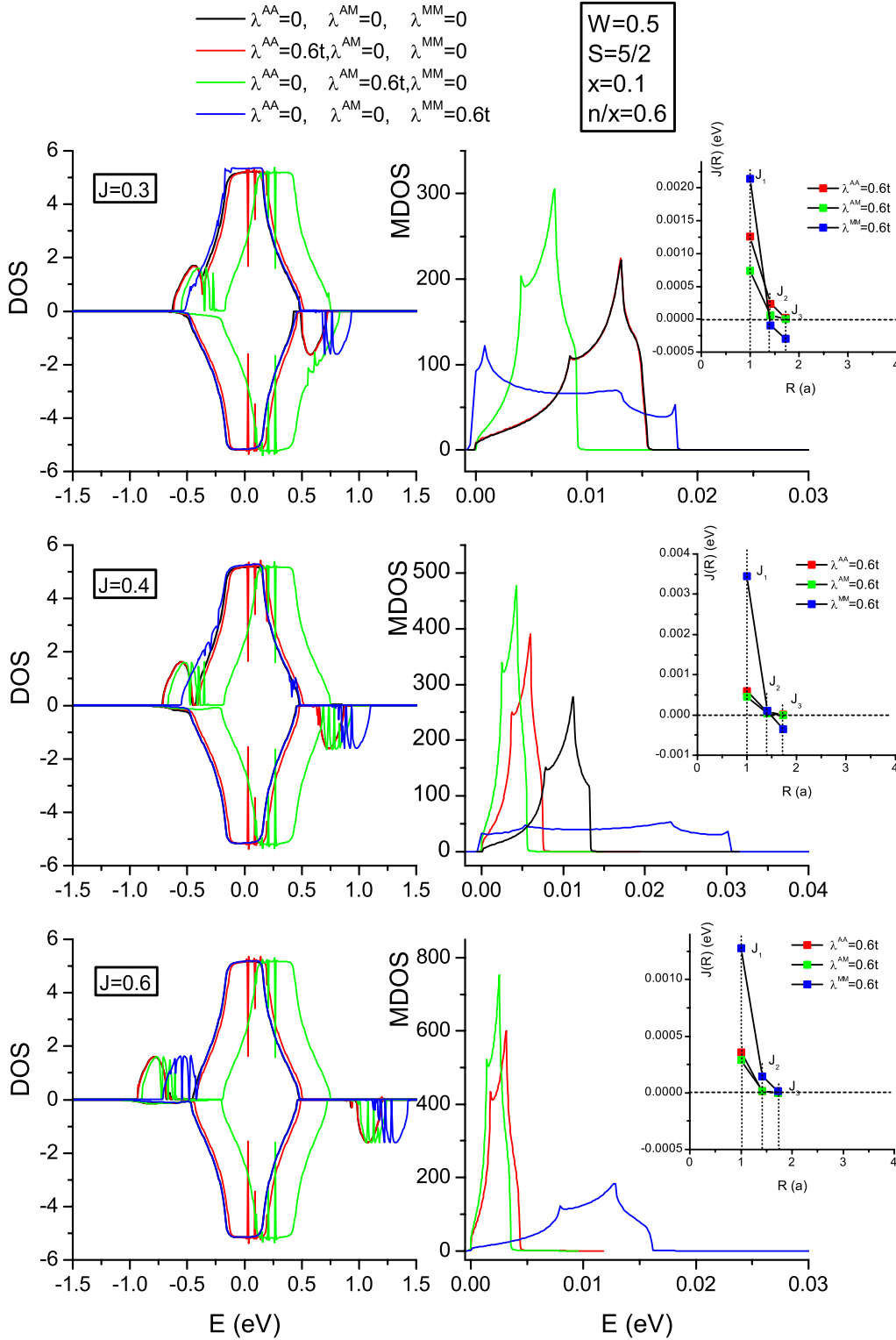


FIG. 2. (Color online) Quasiparticle electron (left column) and magnon (right column) DOS at fixed model parameters $W=0.5$, $S=5/2$, $x=0.1$, and $n/x=0.6$ for three different couplings and for different values of the crystal-field parameters. The inset shows dependence of the MRKKY interaction on the distance R between magnetic atoms in simple-cubic lattice ($R=1$ is a first shell, $R=\sqrt{2}$ is a second shell, and $R=\sqrt{3}$ is a third shell).

oms λ^{AM} plays the role of hybridization between correlated and noncorrelated subbands (green line). At finite temperature all minisubbands are mixed. Finally, the spectrum of up and down electrons from the correlated and noncorrelated

bands becomes symmetric at $T > T_c$, where bands are equally populated and spin-polarization disappears.^{5,6,12,19}

The coupling of the local spins is indirectly being mediated by the itinerant charge carriers via interband exchange

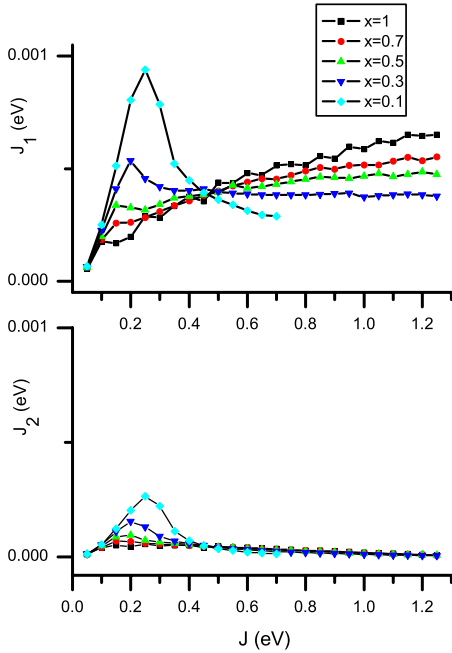


FIG. 3. (Color online) Dependence of the nearest-neighbor effective exchange integral J_1 and the next-nearest-neighbor one J_2 on the exchange coupling J at $W=0.5$ eV, $n=0.06$, $S=5/2$, and $T=0$ for different values of moment concentration x without crystal-field effects.

to the localized moments. So, the electron band concentration n and the concentration x of randomly distributed local moments do strongly influence the character of the long-range exchange interaction J_{ij} between two magnetic atoms M . In the inset of Fig. 2 the change in the MRKKY interaction is shown for the three first shells. Figure 3 exhibits only the dependencies of the effective nearest-neighbor exchange J_1 and next-nearest-neighbor exchange J_2 interaction on the interband exchange coupling J for the case of a switched off crystal field.^{5,6} We identify three regimes for the effective Heisenberg system: low coupling regime with a conventional RKKY behavior $J_1 \sim J^2$; strong coupling regime with short-range interaction J_1 while other exchange integrals J_2, J_3, \dots are small; and the intermediate coupling regime, which plays a very important role for small concentration of magnetic atoms x (see Fig. 3).^{5,6} For the concentrated Kondo-lattice ($x=1$) there is mainly a competition between the low coupling and strong coupling regimes. Enhancing monotonically the exchange coupling J , we can change from free-like regime to the localized one, similar to a double-exchange regime. However for the diluted case ($x < 1$) and especially for the very low concentration x , the magnetic subsystem is not so closed and the competition between the two counteracting tendencies becomes more visible (Fig. 3).

Figure 4 shows the influence on the crucial field effects on the exchange couplings J_1, J_2 of the effective Heisenberg model for low concentration. We see that the biggest influence of the first exchange constant of the effective Heisenberg model appears for the intermediate regime of the interband exchange coupling. The low coupling regime and the strong coupling regime are absolutely the same as for the situation where all crystal-field effects are neglected. The

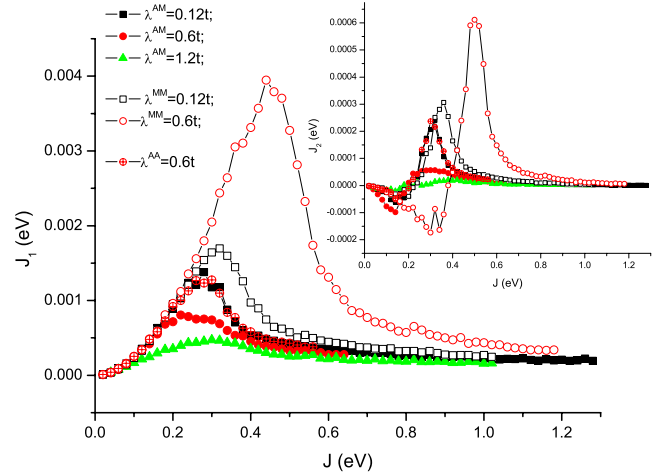


FIG. 4. (Color online) Dependence of the nearest-neighbor effective exchange integral J_1 and the next-nearest-neighbor one J_2 (in the inset) on the exchange coupling J at $W=0.5$ eV, $n=0.06$, $x=0.1$, $S=5/2$, and $T=0$ for different values of the crystal-field parameters λ^{AA} , λ^{AM} , and λ^{MM} .

crystal field λ^{AM} reduces the value of J_1 . The crystal field between two nonmagnetic atoms λ^{AA} does not play any role. Moreover increasing the crystal field between the two magnetic atoms, we can drastically increase the value of the exchange coupling in the effective Heisenberg model.

Such crystal field effects play a critical role for understanding and controlling the ferromagnetic key properties such as the Curie temperature. Figures 5 and 6 show the change in the Curie temperature as function of the interband exchange coupling in the Kondo-lattice model.

Comparing with the concentrated Kondo-lattice model²⁷ ($x=1$), we realize a strong nonmonotonic change in the Curie temperature by a variation of the interband exchange coupling⁵ J (Figs. 5 and 6). This is due, first of all, to the

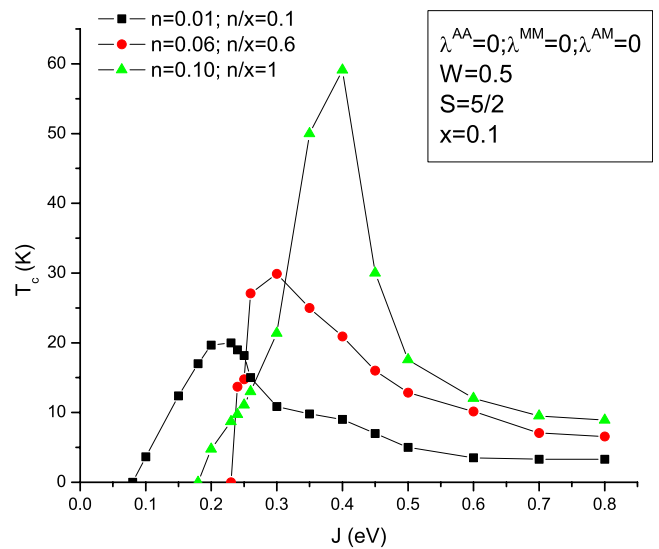


FIG. 5. (Color online) Dependence of the Curie temperature T_c on the exchange coupling J at $W=0.5$ eV, $S=5/2$, and $x=0.1$ and three different value of a small electron concentration $n/x=0.1$, $n/x=0.6$, and $n/x=1$ without crystal-field parameters influence.

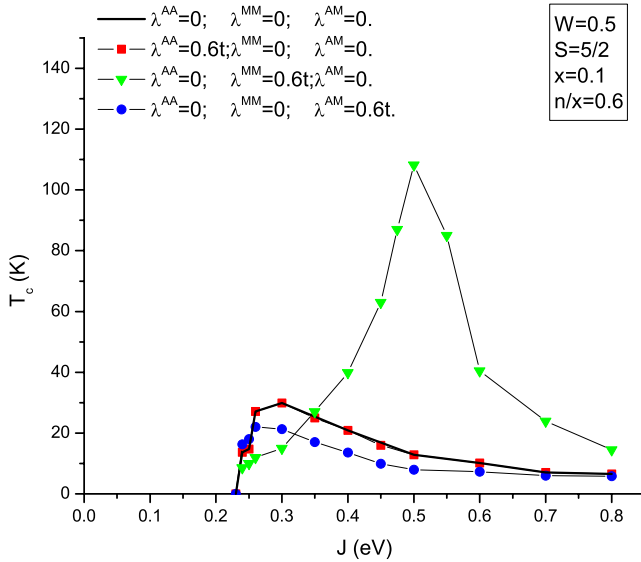


FIG. 6. (Color online) Dependence of the Curie temperature T_c on the exchange coupling J at $W=0.5$ eV, $n=0.06$, $x=0.1$, and $S=5/2$ for the case of finite crystal-field parameters.

effective exchange coupling in the effective Heisenberg model (Fig. 4). However even for an extremely low carrier concentration there is an induced ferromagnetism. The exchange coupling J must exceed a critical value J_c to get a finite T_c . For $J < J_c$ the system has paramagnetic properties ($T_c=0$). For the strong coupling regime the Curie temperature is saturated to some constant value (Fig. 5). It turns out that a realistic effective occupation parameter of the correlated subbands for the diluted Kondo-lattice is the value n/x rather than n . There is also a nonmonotonic shift to higher values of the critical exchange coupling J_c when increasing the electron band occupation n/x as in the concentrated Kondo-lattice model.²⁷

Figure 6 shows the dependence of the Curie temperature on the interband exchange coupling constant J , with included crystal-field effects in the first environment shell (see Fig. 1). We see that the crystal-field effects do not change drastically the Curie temperature in low and strong coupling regimes compared to the case without crystal-field effects. But there is a drastic change in the intermediate region of the interband exchange coupling ($0.3 < J < 0.7$). Especially, increasing the crystal-field parameter between two magnetic atoms λ^{MM} can lead to a very drastic Curie temperature (Fig. 6).

IV. SUMMARY

It is clear that a realistic electronic-structure calculation based on density-functional theory⁸ or numerical methods such as the classical quantum Monte Carlo^{7,10} can give more realistic results. However, the disadvantage of these calculations comes from their strong material dependence and they do not explain the basic physics of disordered local-moment systems in a simple way.

A special challenge when treating the random Kondo-lattice model arises with the fact that both the electron and the spin subsystem have to be considered simultaneously and

on the same level.^{5,6} So, we have performed a self-consistent model calculation of the electronic and magnetic properties of diluted local-moment systems $A_{1-x}M_x$ described by ferromagnetic Kondo-lattice model ($s-f$ model), where we included disorder in the first environment shell by use of crystal-field parameters between two nonmagnetic, one magnetic and nonmagnetic, and two magnetic atoms, respectively, λ^{AA} , λ^{AM} , and λ^{MM} . The electronic self-energy was derived by the Green's function formalism (interpolating self-energy approach) previously developed and tested for the normal KLM (Ref. 19). The CPA treatment had to be generalized to include the crystal-field effects and the resulting self-energy turns out to be dependent on the magnetization of the disordered local-moment system. This quantity was determined by mapping the interband exchange interaction of the KLM on an effective Heisenberg model solved in VCA. Finally we arrived at a closed system of equations, which could be solved self-consistently for the electronic and magnetic properties of the diluted local-moment system.

For performing the investigation of the mutual influence of magnetic correlations and disorder effects in diluted local-moment systems, we introduced phenomenological crystal-field parameters ($\lambda^{AA}, \lambda^{AM}, \lambda^{MM}$). These parameters are acting on of the electronic subsystem of the disordered Kondo-lattice. In principle, they must be calculated by a self-consistent procedure together with the effective exchange Heisenberg constants, for example. But the complexity of the problem did not yet allow us to realize this strategy. From the magnon DOS (Fig. 2) we can conclude that for better fitting of our results to the quantum Monte Carlo calculation¹⁰ it is necessary to support large values of the crystal field between two magnetic atoms λ^{MM} .

The effects of the crystal field from the only magnetic atom was recently discussed in Ref. 21 for the DMS system. These was considered a correlation between the on-site crystal-field potential V_i and the exchange constants in the effective Heisenberg model¹⁶ J_{ij} .

Another important method to introduce the crystal-field effects is based on a nondiagonal hopping term between the different kind of atoms and a matrix technique of Ref. 28. But this technique is more complicated to apply than our technique. We reformulated the crystal-field potential energy into a single-site problem, which makes the problem diagonal and gives a possibility to apply CPA technique, where we included the crystal-field effects and their fluctuations in the binary alloy $A_{1-x}Mn_x$ for the first coordination shell only. In the future we plan also to test this technique for other binary alloys and give a more detailed comparison to standard approaches.^{17,25}

The crystal-field effects play a crucial role for understanding and controlling key-properties such as the Curie temperature. We have seen that disorder effects in the first environment shell had changed the Curie temperature very drastically. In order to compare our model calculation with experimental data such as $Ga_{1-x}Mn_xAs$, we planned to combine our study with realistic parameters from an *ab initio* band-structure calculation.

ACKNOWLEDGMENTS

One of the authors (V.B.) gratefully acknowledges finan-

cial support from the Graduate College of the Deutsche Forschungsgemeinschaft: “Fundamentals and Functionality of Size and Interface Controlled Materials: Spin-and Optoelectronics.”

APPENDIX: ISA TREATMENT

The approximate expressions for the electronic self-energy of the low-density KLM used in the paper are the following:

$$\sum_{\sigma}^{\text{ISA}}(E) = -\frac{1}{2}Jz_{\sigma}\langle S^z \rangle + \frac{1}{4}J^2 \frac{a_{\sigma}G_0(E - \frac{1}{2}Jz_{\sigma}\langle S^z \rangle)}{1 - \frac{1}{2}JG_0(E - \frac{1}{2}Jz_{\sigma}\langle S^z \rangle)},$$

$$G_0(E) = \frac{1}{N} \sum_{\vec{k}} \frac{1}{E - \epsilon(\vec{k})},$$

$$a_{\sigma} = S(S+1) - z_{\sigma}\langle S^z \rangle (z_{\sigma}\langle S^z \rangle + 1),$$

$$z_{\sigma} = \delta_{\sigma\uparrow} - \delta_{\sigma\downarrow}. \quad (\text{A1})$$

This result fulfills the zero-bandwidth limit for all temperatures T and arbitrary coupling strengths J , as well as the exact $T=0$ result for arbitrary bandwidths and couplings (Ref. 19). Exact high-energy expansions helped us to fix the parameters a_{σ} .

-
- ¹J. A. Mydosh, *Spin Glasses: An Experimental Introduction* (Taylor & Francis, London, 1993), p. 256.
- ²T. Jungwirth, Jairo Sinova, J. Masek, J. Kucera, and A. H. MacDonald, *Rev. Mod. Phys.* **78**, 809 (2006).
- ³S. J. Potashnik, K. C. Ku, R. Mahendiran, S. H. Chun, R. F. Wang, N. Samarth, and P. Schiffer, *Phys. Rev. B* **66**, 012408 (2002).
- ⁴C. Zhou, M. P. Kennett, X. Wan, M. Berciu, and R. N. Bhatt, *Phys. Rev. B* **69**, 144419 (2004).
- ⁵G. Tang and W. Nolting, *Phys. Rev. B* **75**, 024426 (2007).
- ⁶V. Bryksa and W. Nolting, *J. Magn. Magn. Mater.* **320**, 699 (2008).
- ⁷A. Singh, A. Datta, S. K. Das, and V. A. Singh, *Phys. Rev. B* **68**, 235208 (2003).
- ⁸J. Kudrnovsky, I. Turek, V. Drchal, F. Maca, P. Weinberger, and P. Bruno, *Phys. Rev. B* **69**, 115208 (2004).
- ⁹G. Bouzerar and P. Bruno, *Phys. Rev. B* **66**, 014410 (2002).
- ¹⁰S. Hilbert and W. Nolting, *Phys. Rev. B* **70**, 165203 (2004).
- ¹¹Masao Takahashi, *Phys. Rev. B* **70**, 035207 (2004).
- ¹²W. Nolting, T. Hickel, A. Ramakanth, G. G. Reddy, and M. Lipowczan, *Phys. Rev. B* **70**, 075207 (2004).
- ¹³Avinash Singh, K. Das Subrat, A. Sharma, and W. Noting, *J. Phys. Condens. Matter* **19**, 236213 (2007); Subrat Kumar Das, Avinash Singh, arXiv:cond-mat/0506523.
- ¹⁴D. J. Priour and S. Das Sarma, *Phys. Rev. Lett.* **97**, 127201 (2006).
- ¹⁵W. Nolting, S. Rex, and Jaya S. Mathi, *J. Phys.: Condens. Matter* **9**, 1301 (1996).
- ¹⁶A. I. Liechtenstein, M. I. Katsnelson, V. P. Antropov, and V. A. Gubanov, *J. Magn. Magn. Mater.* **67**, 65 (1987).
- ¹⁷R. J. Elliott, J. A. Krumhansl, and P. L. Leath, *Rev. Mod. Phys.* **46**, 465 (1974).
- ¹⁸T. Matsubara and F. Yonezawa, *Prog. Theor. Phys.* **34**, 871 (1965).
- ¹⁹W. Nolting, G. G. Reddy, A. Ramakanth, and D. Meyer, *Phys. Rev. B* **64**, 155109 (2001).
- ²⁰W. H. Butler, *Phys. Lett.* **39A**, 203 (1972).
- ²¹R. Bouzerar, G. Bouzerar, and T. Ziman, *Phys. Rev. B* **73**, 024411 (2006).
- ²²H. B. Callen, *Phys. Rev.* **130**, 890 (1963).
- ²³H. Dvey-Aharon and M. Fibich, *Phys. Rev. B* **18**, 3491 (1978).
- ²⁴S. F. Edwards, *Philos. Mag.* **3**, 1020 (1958).
- ²⁵A. I. Gusev, A. A. Rempel, and A. J. Magerl, *Disordered and Order in Strongly Nonstoichiometric Compounds* (Springer, Berlin, 2001), p. 607.
- ²⁶J. M. Ziman, *Models of Disorder* (Cambridge University Press, Cambridge, 1979), p. 591.
- ²⁷C. Santos and W. Nolting, *Phys. Rev. B* **66**, 019901(E) (2002).
- ²⁸J. A. Blackman, D. M. Esterling, and N. F. Berk, *Phys. Rev. B* **4**, 2412 (1971).